Engineering Science & Technology
http://ojs.wiserpub.com/index.php/EST/

UNIVERSAL WISER PUBLISHER

Research Article

Health Monitoring of Storage Tanks Subject to Near-Field and Far-Field Earthquakes

Hossein Mirzaaghabeik*, Rafael Holdorf Lopez, Marcos Souza Lenzi

Center for Optimization and Reliability in Engineering, Civil Engineering Department, Federal University of Santa Catarina, Rua João Pio Duarte Silva, s/n 88040-900 Florianópolis, SC, Brazil
E-mail: hossein_aghabeik@yahoo.com

Received: 14 September 2020; **Revised:** 6 April 2021; **Accepted:** 19 April 2021

Abstract: Structural Health Monitoring (SHM) is a method to conserve the structures and monitor their stress and strain situation. Natural disasters, significantly the earthquake could damage the water supply systems, including water tanks. The earthquake could conclude cavitation and water sloshing inside the underground water tank. On the other hand, it can cause human tragedy economically, socially, and ecologically. Therefore, useful and essential measures for repairing and utilizing the underground water tanks after the earthquake should be considered. This research aims to monitor the underground storage tanks subject to near-field and far-field earthquakes, considering the cavitation effect. In this article, the effect of earthquakes on the underground water tanks, considering the seismic behavior and cavitation effect of the underground tank, will be considered. For considering seismic behavior on the storage tanks and their reaction, the ANSYS software has been used to simulate and model them via the finite element method. After that, the prone places to the cavitation wherever the pressures are minus will be detected by the Monte Carlo method. The cavitation effect statistics were examined, and their placement is compared with the results obtained from the Monte Carlo method. The MATLAB codes have been used to make decisions for optimal smart sensor placement via the Monte-Carlo method. Moreover, to decrease the analysis time, the comparison method is taken into account. Finally, underground water tanks were loaded subjected to near-field and far-field earthquakes. The finite element result will be analyzed via the Monte Carlo method, and the best places for installing the smart sensors will be proposed.

***Keywords*:** storage tank, earthquake, cavitations, Structural Health Monitoring

1. Introduction

For years, knowledge, technology, and art contribute to each other in providing modern and efficient tools, structures, and models, which leads the present modern world towards a situation in which within near future, one can expect fewer surprises by natural disaster making them a part of past. In the age of technology, the speed of changes, innovations, and inventions is so much that one feels the need to learn and share thoughts and information at each moment.

Water tanks are divided into top-ground and underground forms. Due to the significant effect of these structures after an earthquake for shutting down the fire, providing drinking and washing water, they are among highly significant

DOI: https://doi.org/10.37256/est.222021640

structures. Therefore, investigations of these tanks' secure and incessant performance against probable severe earthquakes are fundamental. On the other hand, water in these structures and the problem of analyzing fluid-structure interaction in the seismic analysis is very complicated.

The study of liquid water and hydrodynamic pressure of liquids have a long-term historical background. Fundamental studies on this domain were started in the 1880s. Investigation and analysis of tanks by dampers and optimal placement and geometry of dampers to reduce the effects of cavitation can reduce the seismic damages and prevent seismic damage of tanks.

One of the most important external forces, such as seismic waves on tanks, is water sloshing. The sloshing and changing in the pressure of the water tank can create cavitation phenomena. This fluctuating water level can be made unexpectedly unstable in all systems or even system damages directly or indirectly [1]. As the amplitude of stimulation increases or the system frequency reaches natural turbulence frequency, this phenomenon becomes more apparent. This phenomenon is elementary, but it is a destructive phenomenon (cavitation). It is unpredictable, but today, the prevention methods have turned into highly controversial discussions among associated researchers on fluids mechanics. Figure 1 and Figure 2 illustrate the sloshing water cause of earthquake forces. It ignites the storage tanks cause of fuel cavitation.

Figure 1. Water sloshing cause of earthquake forces

Figure 2. Ignite the storage tanks cause of fuel cavitation

Mirzaaghabeik and Vosoughifar [2] evaluated the Health Safety Environment (HSE) index of the Lightweight Steel Framing (LSF) system subjected to near-and-far field earthquakes. Guerriero et al. [3] studied the problems involved in installing sensors in smart wireless networks. To this end, they defined and investigated various mathematical models for different purposes. Debnath et al. [4] used the results of modal analysis for 1-DoF systems to determine the optimal location for sensors' placement. Chan Bae et al. [5] investigated the effects of different structural components on smart wireless networks' performance. Hao and Oral [6] in 2017 presented a benchmark problem for the structural health

monitoring community to study tall buildings. He et al. [7] in 2014 proposed a time-domain integrated vibration control and health monitoring approach based on the extended Kalman filter (EKF) for identifying the physical parameters of the controlled building structures without the knowledge of the external excitation. He et al. [8] in 2017 experimentally explored the possibility of establishing such a smart building structure with the function of simultaneous damage detection and vibration suppression. Qingkai Kong et al. [9] in 2018 provided an approach to structural health monitoring that it could allow many more commercial and residential buildings to be monitored because it removes the cost-prohibitive nature of traditional seismic arrays and the complexity of deploying the instruments. Ting-Hua et al. [10] conducted a study on sensor placement to monitor high-rise buildings' health using the genetic algorithm (GA). In this study, which also incorporated the message authentication code (MAC) algorithm, the GA was discussed for optimal sensor placement. The researchers proposed a new algorithm allowing a better convergence of the results [10]. Chang and Pakzad [11] studied structural health monitoring through advanced statistical methods and the energy method for modal identification purposes. They used the MAC to correlate the evaluated modes and those obtained using the bridges' finite element models. Mirzaaghabeik and Vosoughifar [12] compared the quality and quantity seismic damage index for the LSF system. Mirzaaghabeik and Vosoughifar [13] also worked on LSF system braces' optimum connection using the seismic-Artificial Neural Network (ANN) approach.

In recent years, to reduce the effects of cavitation and prevent various damages of this phenomenon, different options such as optimization of the tank through advanced computer sciences and smart materials have drawn researchers' attention [14]. This research aims to apply intelligent sensors as one of the modern methods for health monitoring in water tanks. Although the usage of sensors, in this case, is very innovative, due to the high economic costs of using high numbers of them, it isn't economically feasible. For this reason, the use of the Monte Carlo method helped to analyze the appropriate points for the installation of these sensors. Due to this issue that optimization seeks to improve the performance of obtaining optimal points, to ensure economic feasibility and industrial usage, the location of these walls is designed to minimize turbulence.

2. Research method

2.1 *Definition*

First, some water tanks were chosen as samples to do the present study. The selected tanks were modeled by proper Finite Element Model (FEM) software. In this study, static and dynamic analyses were done. In this regard, six earthquakes with distinctive accelerograms were chosen, that three of them were selected from a near field, and the other three were selected from a far-field earthquake. These earthquakes were separately applied to the water tanks. Due to these seismic forces, the inside-the-tanks fluid had sloshing, and in some points, this phenomenon led to the generation of negative pressure due to severity. These points have negative pressure, which results in the generation of cavitation. The locations of cavitations were defined by numerical analysis, and the Monte Carlo method was used to describe the most appropriate points based on a suitable target. More details will be provided in the following.

2.1.1 *Earthquake ground motion*

According to the site land's soil type, three near-field earthquakes and three far-field earthquakes were selected. The near-field earthquakes have been selected considering three essential factors that are below:

1. It has been tried to select the earthquakes that its frequency period is the same as the underground tanks' frequency period.
2. The distance between earthquake record location and earthquake center.
3. The pulse effect in the earthquake spectrum.

The above factors were considered as defining factors to select the near-field earthquakes.

Tables 1 and 2 show the near-field and far-field earthquakes' specifications.

Table 1. The near-field ground motion records that have been used

Earthquake	Record ID	Magnitude (Ms)	PGA (g)	Epicentral distance (km)
Tabas (1978)	P0144	7.4	0.81	5
Northridge (1994)	P0887	6.7	0.32	3
Nahanni (1985)	P0336	6.6	0.55	6

Table 2. The far-field ground motion records that have been used

Earthquake	Record ID	Magnitude (Ms)	PGA (g)	Epicentral distance (km)
Sanfernando (1971)	P0056	6.6	0.29	25
Kobe (1995)	P1041	6.9	0.26	33
Santa Barbara (1978)	P0256	5.8	0.25	27

2.2 *Case study selection process*

A few parameters should be considered to investigate water tanks subjected to the time-acceleration effect of near- and far-field seismic waves. These parameters include optimal definition dimensions and selecting the proper seismic waves for stimulating and the number of forces that affected the water tank. Many researchers have been done in this domain, and the information presented in the American Petroleum Institute (API) standard, the optimum dimension of the reservoir was selected [15]. According to the mentioned standard for the case study, a 10.000 cubic-meter twin water tank was selected. The economic height of this case study, according to the mentioned standard, is 5 meters. The geometry of tanks based on economic parameters was inserted in Table 3.

Table 3. Optimum geometry of water tank based on economic consideration

Volume of storage (m^3)	Length (m)	Water height (m)
2000	3.8	4
5000	4	5
10000	5	(5-6)
15000	(5-6)	6
20000	(5-6)	6

Table 4. Specification of various case studies

Volume of storage (m^3)	Length (m)	Width (m)	Height (m)	Water height (m)
5000	32	22	7	6.7
2000	25	18	4.5	4.2
1000	21	12	4	3.8
500	16	10	3	2.8
320	16	10	2	1.8

The ideal dimension of the reservoir with the desired volume can be defined via Table 1. In this regard, the specification of various reservoirs was investigated as case studies in this research. The specification of these reservoirs is given in Table 4.

3. Modeling

3.1 *Finite Element Model (FEM)*

To model the reservoir using the finite element method and consider the structure's interaction and the liquid has been used. The displacement of the node in the structure and the fluid environment has been unknown. And deals with the history of a particle over time and forms a system of symmetric coordinate equations. For this purpose, the ANSYS finite element program has been used. For the fluid, an 8-node, three-dimensional element with 24 degrees of freedom (3 degrees of freedom of movement per node) was used. For this element, the fluid elasticity modulus was taken according to the fluid bulk modulus. The stress-strain relationship is defined as follows.

$$P = E \times \varepsilon\_bulk \tag{1}$$

Where P is the pressure and ε_bulk is the element strain. Incompressible fluid $E = 2.1\times 10^6$ (Kpa) and the density $\rho = 1000$ (kg/m^3) are considered. For tank walls, a three-dimensional 8-node structural element with 24 degrees of freedom (3 degrees of freedom of displacement per node) is used, and $E = 22.69$ (Gpa) and density $\rho = 2400$ (kg/m^3) is considered. Displacement of structural and fluid nodes in the structure environment and fluid is connected perpendicular to the surface. It means that fluid and structure can't be separated from each other; instead, they move perpendicularly to the plane, which satisfies Hans's assumptions, which he considered in his simplified mechanical model. Also, to create an integrated system and prevent the walls from moving independently, degrees of freedom to move the node above the wall are connected.

3.2 *Validation with laboratory results*

A laboratory model conducted by Goodarzi et al. [16] in 2009 at the University of Stuttgart, Germany, is used to validate the finite element components and results model. This laboratory model is a rectangular tank with dimensions of 1 × 0.4 × 0.96 (length × width × height) with a water height inside the tank equal to 0.624 meters on a vibrating table with dimensions of 1 × 2 meters.

Which is under the harmonic sine vibration obtained from Equation (2) with the angular frequency more significant than the first natural frequency of the fluid obtained from Equation (3) with a ratio of $\frac{\omega_1}{\omega_2} = 1.12$.

The fluid's maximum turbulence height in the experimental model is 62.3 mm, and the first to third natural frequency modes of the fluid from the analytical ratio 3 are 0.886, 1.562, and 2.017 Hz, respectively. For optimal meshing in the finite element method, 12 types of banding elements with different sizes were used, summarized in Table 5 of the number of elements and the finite element method results. Figure 3 shows the mesh modeling of the case study via a powerful FEM approach.

$$X_{(t)} = D\sin(\omega t) \tag{2}$$

$$\omega_n{}^2 = \pi(2n-1)\left(\frac{g}{L}\right)\tanh\left[(2n-1)\left(\frac{h}{L}\right)\right] \tag{3}$$

In Equation (2), (D) is the maximum horizontal displacement of the reservoir, which is considered to be 0.005 meters. In Equation (3), (n) is the oscillation mode number, and (L) is the reservoir's length.

Table 5. Characteristics of different types of laboratory tank elements with different dimensions and summary of results obtained by finite element method

Type of element	Number of elements			Number of fluid elements	Mods derived from FEM (HZ)			Maximum Sloshing Wave Height (mm)	Percentage of total turbulence with SPSS
	Height (m)	Length (m)	Width (m)		First mode	Second mode	Third mod		
1	2	5	2	20	0.832	1.089	-	37.7	38%
2	3	5	2	30	0.859	1.306	-	48.3	62%
3	4	5	2	40	0.871	1.447	-	56.8	71%
4	6	5	2	60	0.879	1.613	-	64.3	51%
5	3	10	4	120	0.849	1.23	1.317	46.2	56%
6	4	10	4	160	0.860	1.34	1.503	51.7	68%
7	6	10	4	240	0.868	1.452	1.750	58.3	78%
8	8	10	4	320	0.871	1.502	1.900	60.3	76%
9	12	10	4	480	0.873	1.543	2.049	63.7	65%
10	8	20	8	1280	0.868	1.465	1.791	60.9	72%
11	12	20	8	1920	0.870	1.503	1.907	60.3	75%
12	25	38	16	15200	0.870	1.515	1.951	62.35	73%

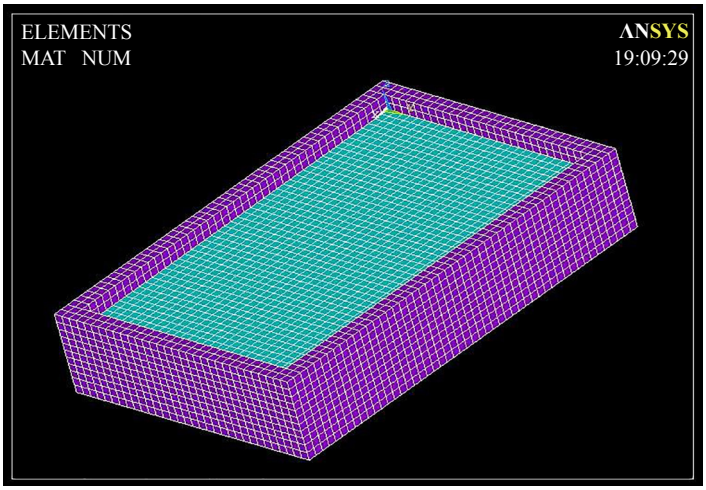

Figure 3. Mesh modeling of case study via a powerful FEM approach

Figure 4 also shows the time history of some of the finite element method elements compared to the time history of the free surface turbulence of the laboratory method's liquid. Figure 5 shows the seismic sloshing modeling of the water tank by proper FEM software.

The modal analysis results show: oscillatory modes, especially in the first mode, do not differ much from each other and become homogeneous as the number of elements decreases by one number. If the maximum turbulence differs from the analysis of time history, therefore, it must also consider higher modes to validate the element's behavior.

The size of larger elements cannot be calculated and also higher modes cannot be calculated-which can be affected in an earthquake (Table 5-Types 1 to 4).

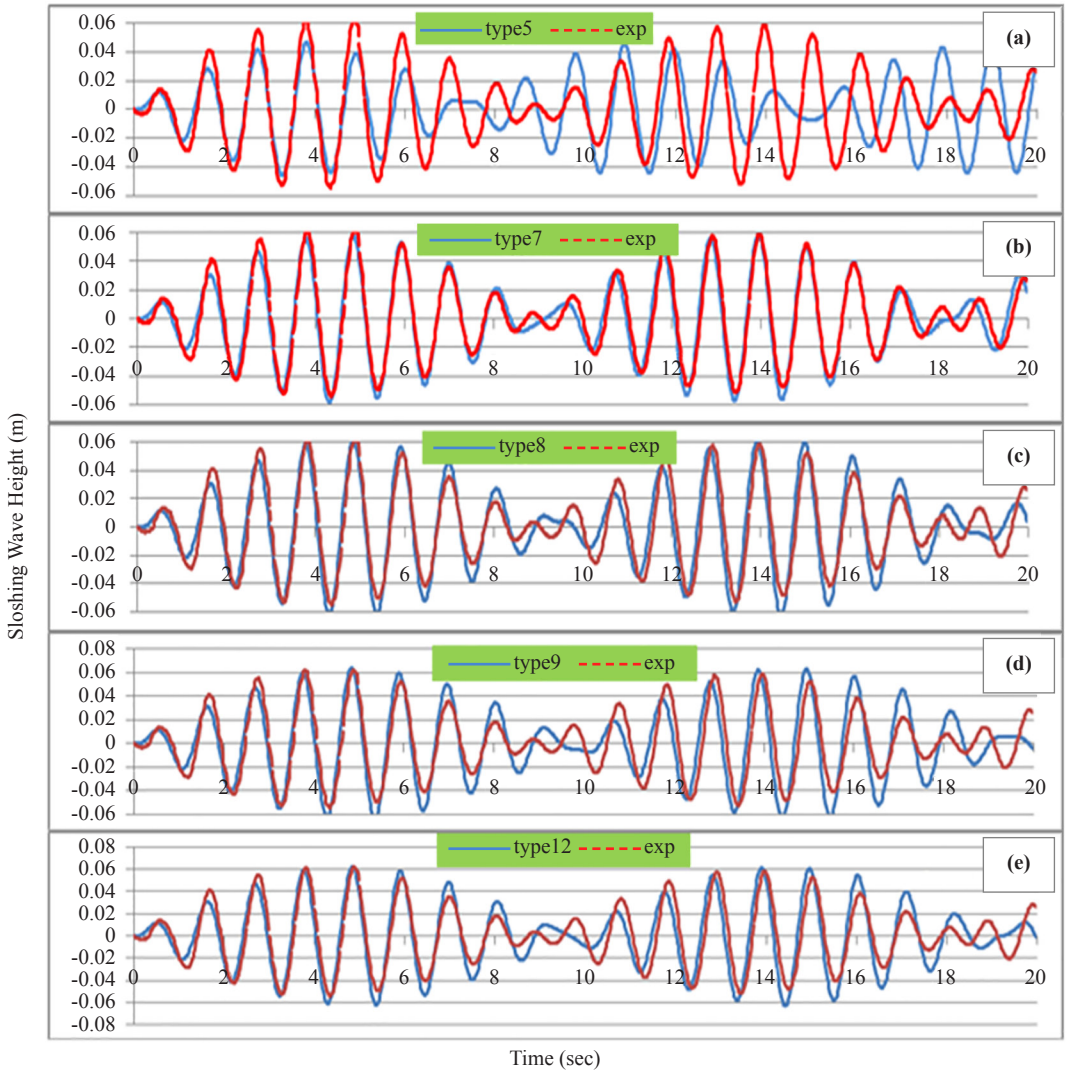

Figure 4. Comparison between experimental results with a finite element method with different element sizes for turbulence height over time.

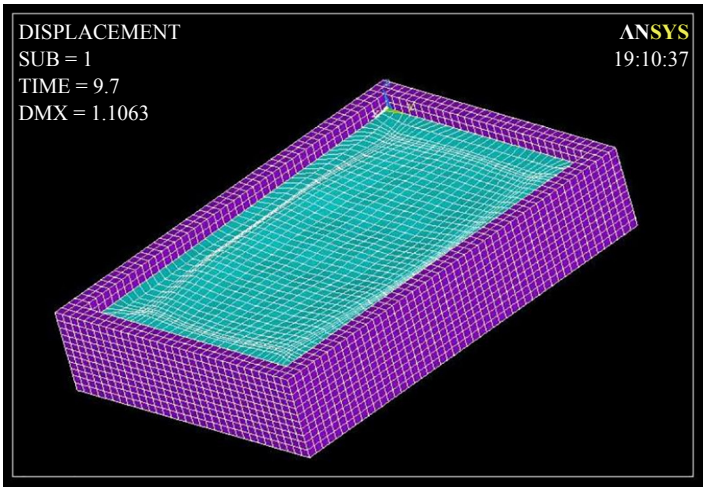

Figure 5. Shows the seismic sloshing modeling of the water tank by proper FEM software.

Table 5 shows that it is essential to decrease the element's height with constant length and width dimensions (types 1 to 4, 5 to 9, 10, and 11) the oscillation modes and the fluid's maximum height turbulence increase. (Figures 4-a to 4-d) And elements with a height-to-width ratio greater than one show maximum less turbulence and phase change. As a result, the fluid's free surface turbulence trend over time is entirely different from the experimental results (Figure 2-a) and square cube elements. A height-to-width ratio of less than 1 gives better and maximum turbulence results closer to the test results.

However, by greatly reducing the elevation relative to the width or further shrinking all dimensions of the element, the turbulence process over time differs from the experimental results. And due to the linear method of the finite element components, the minimum fluid surface turbulence makes a greater difference than the laboratory results (Figures 4-d and 4-e). With the SPSS17 statistical program, the results obtained from different elements and laboratory results have been compared to the Mann-Whitney test, which confirms the above results. (P-Value = 0.619 > 0.05)

3.3 *The effect of the element on the dynamic analysis of reservoirs*

For dynamic analysis, a reservoir with dimensions of 14 × 18 × 5 (m) with a water height of 4 (m) and a volume of 1000 m^3 has been considered. The model has been done according to the method described in section 3. Figure 6 shows the type 7 element with dimensions of 1 × 1 × 0.8 (m). According to the previous section's element results, elements with a height-to-width ratio greater than one and much smaller than one cause a phase change in the results and maximum turbulence. The eight types of elements have been used for analyzing the actual reservoir's sensitivity by considering the optimal element. It should be noted that the ratio of the height to width of the mentioned elements is about 0.75. The modal analysis has been performed for them. The results and fluid turbulence modes obtained from Analytical Equation (3) are given in Table 6.

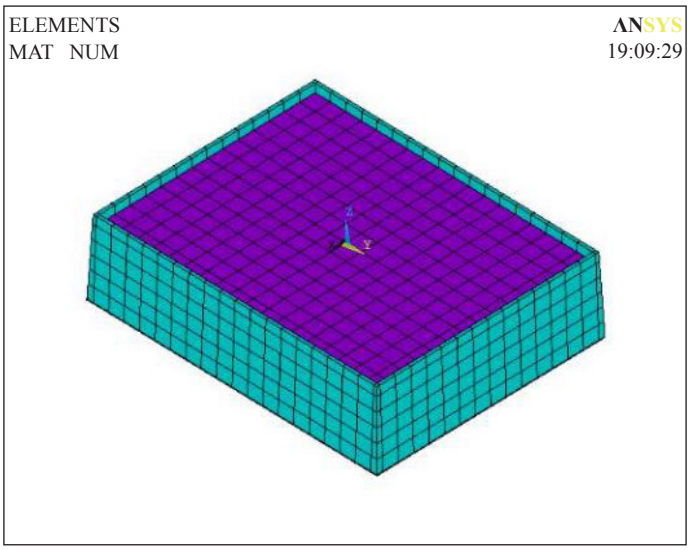

Figure 6. The type seven-element with dimensions of 1×1× 0.8 (m)

As shown in Table 6, the modes obtained from different elements (especially in the first mode) are not very different and should consider higher modes to determine the optimal size range.

Modal analysis and harmonic analysis show that elements with a height-to-width ratio of about 0.75 result in greater maximum turbulence than cubic elements. It gets closer to the results of a smaller cube element. To reduce the elements and reduce the volume of operations, we can use elements with a lower height-to-width ratio and as mentioned, this ratio should not be too small.

Table 6. Characteristics of different types of 1000 cubic meter tank elements with different dimensions of elements and turbulence modes obtained from these elements

Element size (Length × width × height) (m)		Type of element							
		3 × 3 × 2	2 × 2 × 2	2 × 2 × 1	1.4 × 1.5 × 1.4	1.4 × 1.5 × 1	1 × 1 × 1	1 × 1 × 0.8	0.5 × 0.5 × 0.5
Mode	Analytical modes	Type 1	Type 2	Type 3	Type 4	Type 5	Type 6	Type 7	Type 8
1	0.1617	0.1631	0.1614	0.1624	0.1615	0.1618	0.1614	0.1615	0.1614
2	0.3552	0.3603	0.3411	0.3599	0.3471	0.3520	0.3467	0.3489	0.3481
3	0.4651	0.4460	0.4061	0.4841	0.4387	0.4594	0.4445	0.4537	0.4546
4	0.5509	-	0.4436	0.6033	0.4956	0.5406	0.5049	0.5255	0.5270

The relationship among hydrodynamic, hydrostatic, and atmosphere pressures has been evaluated. If the liquid pressure calculated via Equation (4) becomes negative, cavitation has occurred. Figure 7 to Figure 10 show this issue. According to the various colors in the mentioned figures, the red color shows a higher possibility of cavitation.

$$(P_{Hydrodynamic\ pressure} + P_{Hydrostatic\ pressure} + P_{atm})\ center\ of\ its\ Fluid\ Element \leq 0 \tag{4}$$

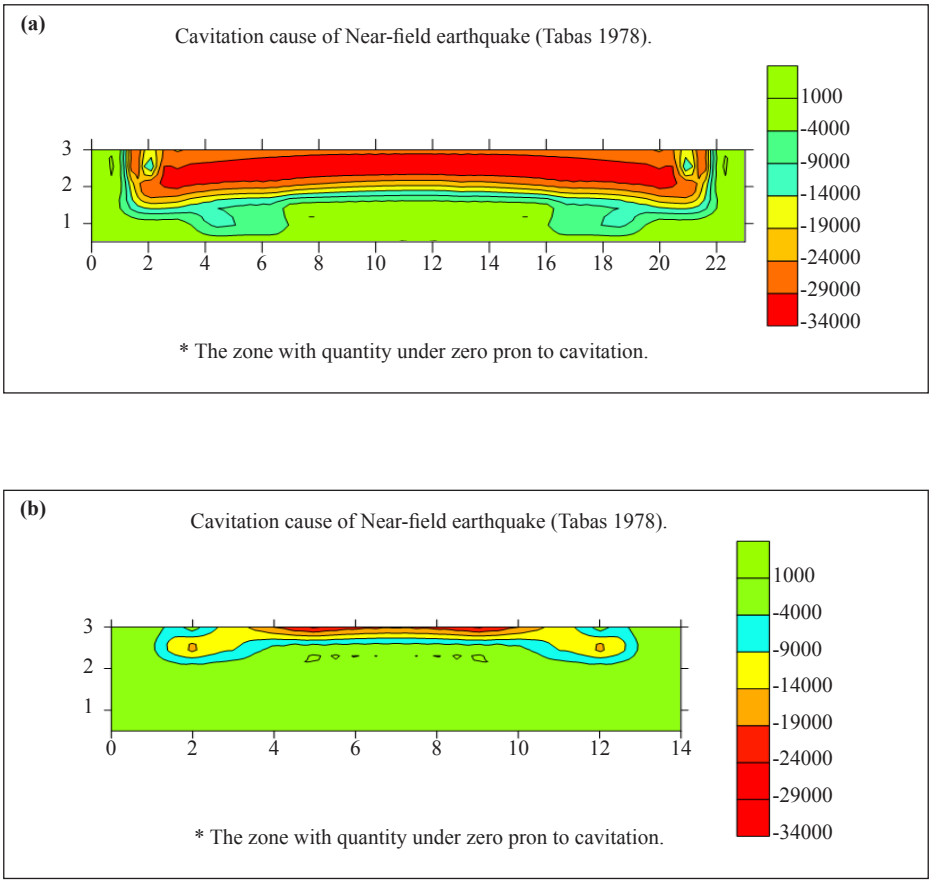

Figure 7. Near-field earthquake Tabas (1978) for the longitudinal (a) and the transverse (b) walls of the tank

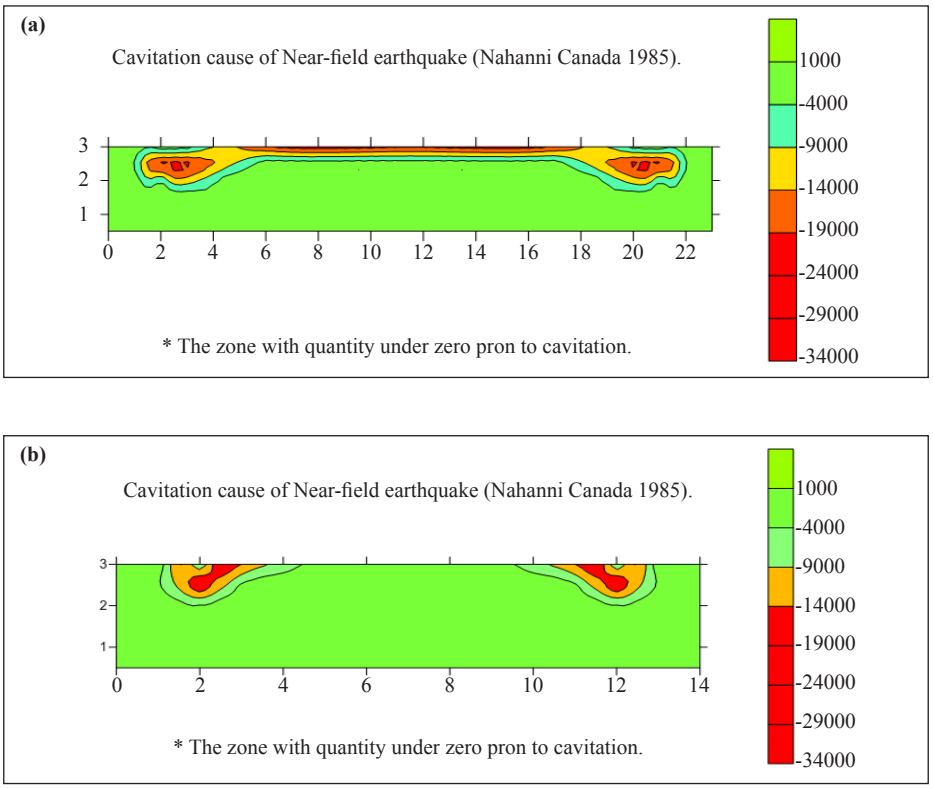

Figure 8. Near-field earthquake Nahanni (1985) for the longitudinal (a) and the transverse (b) walls of the tank

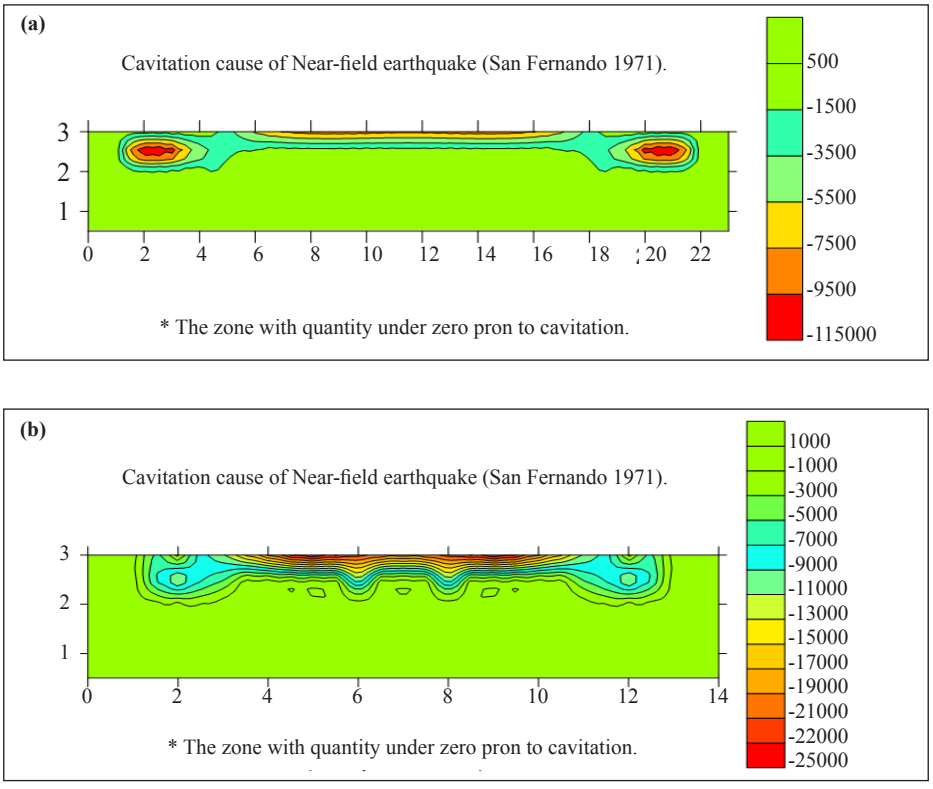

Figure 9. Far-field earthquake San Fernando (1971) for the longitudinal (a) and the transverse (b) walls of the tank

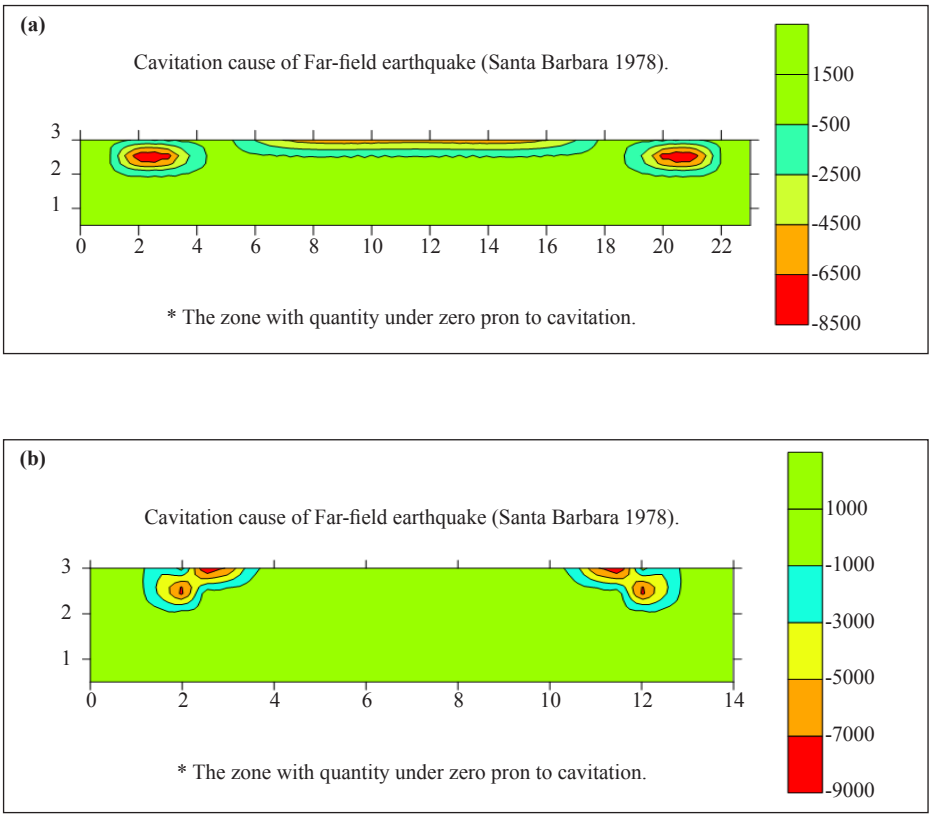

Figure 10. Far-field earthquake Santa Barbara (1978) for the longitudinal (a) and the transverse (b) walls of the tank

Due to the above figures, there is a significant difference in cavitation location in far-field and near-field. Near-field earthquakes have vertical seismic acceleration, and there is a high possibility of cavitation in this field compared with far-field ones.

4. Optimal placement of smart sensors

4.1 *Neural networks*

Optimal placement of smart sensors was obtained with the processing of the neural network. In this process, the non-linear equation between coordinated points and displacement value calculated via various types of the earthquake was created. In this network, x and y data are used as input variables as coordinate points. Negative pressure was defined as an objective function after creating a neural network; the non-linear relationship was established between input and output. In this research, two optimal layers were defined for the neural network. A tangent sigmoid function was defined as the first layer, and for the second layer, Purline linear function was selected. To get the intended result Mean Squared Error (MSE) approach was applied. This approach was designed for controlling minimum error as given in Equation (5). Figure 11 shows the optimal neural network layers with two layers.

$$MSE = \frac{1}{N}\sum_{i=1}^{N}(y_i - \acute{y})^2 \tag{5}$$

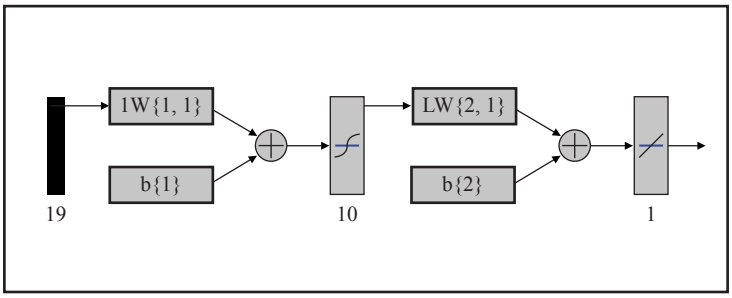

Figure 11. Optimal neural network layers with two layers

To better evaluate optimal network selection performance, the correlation coefficient was selected as a proper approach to comparing initial displacement data, and obtained values computed from the non-linear equation by the mentioned coefficient show the best correction of about 0.998.

Therefore, the selected layer can be used as an optimal non-linear equation for defining the seismic displacement of water tanks. This equation is given by Equation (6).

$$dif\ f = w_2 * \left[\frac{1-\exp(-2(w_1 I + b_1))}{1+\exp(-2(w_1 I + b_1))}\right] + b_2 \tag{6}$$

Artificial Neural Networks (ANNs) are suitable mathematical tools that emulate from biological neuron system. Neural Networks have high flexibility and correction in adaptation with existing data to find the arrangement and association with their definite organization.

4.2 *Monte carlo method*

In general terms, the Monte Carlo method (or Monte Carlo simulation) can be used to describe any technique that approximates solutions to quantitative problems through statistical sampling. As used here, 'Monte Carlo simulation' is more specifically used to describe a method for propagating (translating) uncertainties in model inputs into uncertainties in model outputs (results). Hence, it is a type of simulation that explicitly and quantitatively represents uncertainties. Monte Carlo simulation relies on the process of explicitly representing uncertainties by specifying inputs. If the inputs describing a system are uncertain, the prediction of future performance is necessarily uncertain. The result of any analysis based on inputs represented by probability distributions is itself a probability distribution. Flow is a derived measurement that is invariably obtained from several measurements with a functional relationship that must be considered when analyzing the measurement uncertainty. These relationships are often complex, and frequently the results are input into a larger measurement system. The Root Sum Square (RSS) method's conventional uncertainty analysis is often difficult in complex systems. It requires approximation at each stage of processing, placing serious doubts on the validity of the results. Recent developments in the analysis of uncertainty using Monte Carlo Simulation (MCS) have resolved many problems. These include non-symmetric measurement uncertainty distributions, non-linearity within the measurement system, input dependency, and systematic bias. The paper is divided into two parts. The conventional estimation methods methodology can be illustrated using a simple measurement equation with y as a continuous function. Y is approximated using a polynomial approximation or an order of Taylor's series expansion. This matter is given by Equation (7).

$$y = f(\bar{x}_1, \bar{x}_2) + \frac{\partial f}{\partial x_1}(x_1 - \bar{x}_1) + \frac{\partial f}{\partial x_2}(x_2 - \bar{x}_2) + W \tag{7}$$

Where $\bar{x}_1, \bar{x}_2$ are mean observed values, and W is defined as Equation (8).

$$W = \frac{1}{2!}\left[\frac{\partial^2 f}{\partial x_1^2}(x_1 - \bar{x}_1)^2 + \frac{\partial^2 f}{\partial x_2^2}(x_2 - \bar{x}_2)^2 + 2\frac{\partial^2 f}{\partial x_1 \partial x_2}(x_1 - \bar{x}_1)(x_2 - \bar{x}_2)\right] \quad (8)$$

As the partial derivatives are computed at the mean value $\bar{x}_1, \bar{x}_2$, they are the same for all $i = 1, \ldots, N$. All the higher terms are normally neglected, and Equation (7) becomes Equation (9).

$$y = f(\bar{x}_1, \bar{x}_2) + \frac{\partial f}{\partial x_1}(x_1 - \bar{x}_1) + \frac{\partial f}{\partial x_2}(x_2 - \bar{x}_2) + \frac{1}{2!}\left[\frac{\partial^2 f}{\partial x_1^2}(x_1 - \bar{x}_1)^2 + \frac{\partial^2 f}{\partial x_2^2}(x_2 - \bar{x}_2)^2 + 2\partial^2 f \partial x_1 \partial x_2 x_1 - x_1 x_2 - x_2\right] \quad (9)$$

This is acceptable provided that the uncertainties in x_1 and x_2 are small and all values of x_1 and x_2 are close to $\bar{x}_1, \bar{x}_2$, respectively. Additionally, if f $(x_1, x_2) + \frac{\partial f}{\partial x_1}$ is a linear function, the second-order partial derivatives in Equation (8) are zero, so the remainder, both linearity, and small uncertainty, are prerequisites of the conventional method of uncertainty estimation described below.

The standard deviations ∂x_1 and ∂x_2 are referred to, by the Guide to the Expression of Uncertainty in Measurement (GUM), as the standard uncertainties associated with the input estimates x_1 and x_2. The standard uncertainty in y and can be obtained by Taylor:

$$u(y) = \sqrt{\frac{1}{n}\sum_{i=1}^{N}(y_i - y)} = \sqrt{(\frac{\partial f}{\partial x_1})^2 S(x_1)^2 + (\frac{\partial f}{\partial x_2})^2 S(x_2)^2 + 2\frac{\partial f}{\partial x_1}\frac{\partial f}{\partial x_2}S(x_1, x_2)} \quad (10)$$

5. Results

The validation analysis results showed: elements with a higher height to width ratio cause the phase change and the reduction of the maximum free surface turbulence of the fluid relative to the experimental results.

When the ratio of height to width of the element decreases, the maximum turbulence of the free surface of the fluid increases and becomes closer to the experimental results; however, decreasing the height to width ratio due to the linear analysis causes a more decrease in fluid surface relative to the laboratory results, and the turbulence rate of the fluid varies over time with the laboratory results.

The results of free fluid surface turbulence with different elements were compared with the experimental results by the SPSS17 statistical program. The result showed when the element becomes much smaller, or the ratio of height to width decreases significantly; the turbulence trend varies with the laboratory turbulence trend.

6. Discussion

The finite element analysis of the main equations of sloshing was done in the first step of this research. The sloshing frequency, as an essential value, should be calculated in this step. Due to the complexity of these equations, the numerical approach was used to analyze cavitation. In the research, ANSYS software was used as powerful software to modeling the finite element domain. The seismic analysis of near and far-field earthquake waves was done. In this regard, seismic time history regarding three near-field and three far-field earthquakes was selected and scaled on the research area. As the reservoir analysis results for different seismic time history records, the cavitation locations were found as the present study's objective. After finding the analysis results by ANSYS software, the cavitation positions of points occurred, investigating results, and verifying their accuracy by comparing laboratory samples and controlling optimization through the Monte Carlo algorithm. The optimal placement results by the Monte Carlo method to locate the intelligent sensor on the reservoir walls have been shown graphically with the following figures. Figure 12 shows

the Optimal placement of smart sensors in the storage wall's longitudinal and lateral axis.

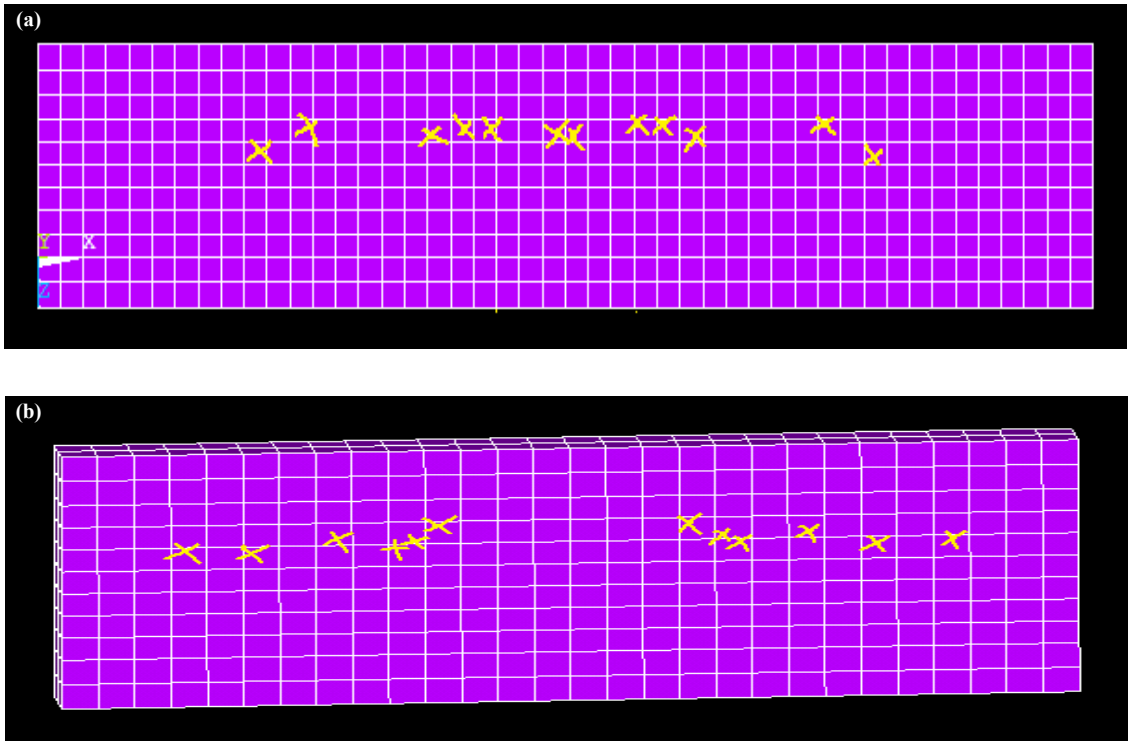

Figure 12. Optimal placement of smart sensors in the the longitudinal (a) and the lateral (b) axis of the storage wall

7. Conclusions

In the present study, an analysis of seismic forces' effects on water containers' fluid was done. After that, the cavitation phenomenon, which intensifies due to the impact of fluid on reservoir walls and damages the reservoir, was investigated. The Monte Carlo algorithm was used to show optimal placement in which it is possible to witness cavitation. Because water tanks usually have a rectangular shape with concrete material, walls were assumed inflexible, and fluid was assumed as an incompressible fluid. The equation's stability values, the time step's value, and the computation steps were considered for defining the numerical analysis elements' suitable values. In estimation, the number of about 19,000 meshes was selected as the optimal value. Validations of the present research were done based on laboratory studies. Statistical analysis between numerical and laboratory results shows no significant difference between them (P-Value < 0.05). The Monte Carlo Approach was applied as proper decision-making for the probability of cavitation location considering sloshing and changing the water tank's pressure. Investigation on the deformation of water surface and value of pressure in different levels on walls shows that the point of pressure measurement to the water surface and remote from corners will increase the possibility of cavitation. The input information and target values must be normalized for generating a non-linear relationship using a neural network. Characteristics of the earthquake, length and width of the water tank, and water tank pressure were defined as objectives or neural networks. Optimal Tangent sigmoid transfer was selected as the first layer or hidden layer of the neural network. For the second layer, after optimal analysis of various layers, the Purline transfer function was selected. The number of the neirons is about 10..

Conflict of interest

The authors declare that there is no conflict of interest regarding the publication of this paper.

Reference

[1] J. H. LEE, J. M. HAN, H. G. PARK, and J. S. SEO, "Improvements of model test method for cavitation-include pressure fluctuation in marine propeller," *Journal of Hydrodynamics, Ser. B*, vol. 25, no. 4, pp. 599-605, 2013.

[2] H. Mirzaaghabeik, and H. R. Vosoughifar, "Evaluation HSE of a LSF system subject to near-and far-field earthquakes," *Pacific Science Review A: Natural Science and Engineering*, vol. 17, no. 3, pp. 69-78, 2015.

[3] F. Guerriero, A. Violi, E. Natalizio, V. Loscri, and C. Costanzo, "Modelling and solving optimal placement problems in wireless sensor networks," *Applied Mathematical Modelling*, vol. 35, no. 1, pp. 230-241, 2011.

[4] N. Debnath, A. Dutta, and S. Deb, "Placement of sensors in operational modal analysis for truss bridges," *Mechanical Systems and Signal Processing*, vol. 31, pp. 196-216, 2012.

[5] B. Sun-Chan, J. Won-Suk, W. Sungkwon, and S. Do Hyoung, "Prediction of WSN placement for bridge health monitoring based on material characteristics," *Automation in Construction*, vol. 35, pp. 18-27, 2013.

[6] S. Hao B. Oral, "The MIT Green Building benchmark problem for structural Health monitoring of tall buildings," *Struct Control Health Monit*, vol. 25, no. 3, pp. e2115, 2018.

[7] J. He, Q. Huang, and X. You-Lin, "Synthesis of vibration control and health monitoring of Building structures under unknown excitation," *Smart Materials and Structures*, vol. 23, no. 10, pp. 105025, 2014.

[8] J. He, X. You-Lin, Z. Sheng, and H. Qin, "Structural control and health monitoring of building structures with unknown ground excitations: Experimental investigation," *Journal of Sound and Vibration*, vol. 390, pp. 23-38, 2017.

[9] Q. Kong, R. M. Allen, M. D. Kohler, T. H. Heaton, and J. Bunn, "Structural health monitoring of buildings using smartphone sensors," *Seismological Research Letters*, vol. 89, no. 2A, pp. 594-602, 2018.

[10] Y. Ting-Hua, L. Hong-Nan, and G. Ming, "Optimal sensor placement for health monitoring of high rise structure based on genetic algorithm," *Mathematical Problems in Engineering*, vol. 22, no. 4, pp. 667-681, 2015.

[11] S. M. A. M. Chang, and A. M. A. S. N. Pakzad, "Optimal sensor placement for modal identification of bridge systems considering number of sensing nodes," *Journal of Bridge Engineering*, vol. 19, no. 6, pp. 1943-5592, 2014.

[12] H. Mirzaaghabeik, and H. R. Vosoughifar, "Comparison between quality and quantity seismic damage index for LSF system," *Engineering Science and Technology, an International Journal*, vol. 19, no. 1, pp. 497-510, 2016.

[13] H. Mirzaaghabeik, and H. R. Vosoughifar, "Optimum connection of LSF system braces using the seismic ANN approach," *Pacific Science Review A: Natural Science and Engineering*, vol. 18, no. 3, pp. 222-227, 2016.

[14] T. Fourest, J. M. Laurens, E. Deletombe, J. Dupas, and M. Arrigoni, "Analysis of bubbles dynamic created by Hydradynamic Ram in confined geometrics using the Rayleigh-Plesset equation," *International Journal of Impact Engineering*, vol. 73, pp. 66-74, 2014.

[15] J. Nazmi, M. Arnaldo, B. Ricardo, *Recommended Practice for Planning, Designing and Constructing Fixed Offshore Platforms*, Working Stress Design API Recommended Practice 2A WSD (RP 2A-Wsd) Twenty-First Edition, 2000.

[16] M. A. Goudarzi, S. R. Sabbagh-Yazdi, and W. Marx. "Investigation of sloshing damping inbaffled rectangular tanks subjected to the dynamic excitation." *Bulletin of Earthquake Engineering*, vol. 8, no. 4, pp.1055-1072, 2010.